Master thesis J.G.V. van Ramshorst

2nd of July 2018

This master thesis is written in the form of a scientific paper for the MSc graduation of J.G.V. van Ramshorst. It is written as a paper, as the aim is to publish the thesis content after the summer. The co-authors have contributed to the results presented in this thesis and will be co-author when the content will be published. The graduation committee contains the following academic staff at Delft University of Technology: A.M.J. Coenders-Gerrits (chair), B. Schilperoort, H.H.G. Savenije (Water Resources) and B.J.H. van de Wiel (Geoscience and Remote Sensing).

To specifically cite this MSc thesis, use the reference link from the TU Delft repository, otherwise refer to the published paper.

Delft, July 2018,

Justus van Ramshorst

Author: J.G.V. van Ramshorst (TU Delft, Water Resources, MSc student)
Co-authors:
A.M.J. Coenders-Gerrits, B. Schilperoort, H.H.G. Savenije (TU Delft, Water Resources)
B.J.H. van de Wiel, J.G. Izett (TU Delft, Geoscience and Remote Sensing)
J.S. Selker, C.W. Higgins (OSU, Biological and Ecological Engineering)

Wind speed measurements using distributed fiber optics: a wind tunnel study

TU Delft

Oregon State University

Abstract

Near-surface wind speed is typically only measured by point observations. The so-called Actively Heated Fiber-Optic (AHFO) technique, however, has the potential to provide high-resolution distributed observations, allowing for better understanding of different processes. However, before it can be widely used, its performance needs to be tested in a range of settings. Therefore, in this work, experimental results on this novel observational wind-probing technique are presented. We utilized a controlled wind-tunnel setup to assess both the accuracy and the precision of AHFO as well as its potential for outdoor atmospheric operation. The technique allows for wind speed characterization with a spatial resolution of 0.3 m on a 1 s time scale. The flow in the wind tunnel is varied in a controlled manner, such that the mean wind, ranges between 1 and 17 ms^{-1}. Comparison of the AHFO measurements with observations from a sonic anemometer shows a high overall correlation, ranging from 0.94-0.99. Also, both precision and accuracy are greater than 95 %. As such, it is concluded that the AHFO has potential to be employed as an outdoor observational technique in addition to existing techniques. In particular, it allows for characterization of spatial varying fields of mean wind in complex terrain, such as in canopy flows or in sloping terrain. In the future the technique could be combined with regular Distributed Temperature Sensing (DTS) for turbulent heat flux estimation in micrometeorological/hydrological applications.

1. Introduction

This work presents the results of a wind study designed to extensively test the novel Active Heated Fiber-Optic (AHFO) wind speed measurement technique in controlled airflow conditions. The primary aims of the experiment were to assess the directional sensitivity and signal-to-noise ratio of AHFO.

Wind speed is most commonly observed using in-situ point measurement techniques. As a result, the spatial distribution of field observations is limited. While it is possible to obtain distributed wind speed observations with remote sensing (e.g., Goodberlet, Swift and Wilkerson, 1989), the spatial resolution is too low for micrometeorological applications. As long as the experimental field site is homogenous, it is possible to use Taylor's frozen flow hypothesis, (Taylor, 1938), to estimate fluxes with the similarity theory, as is done in a lot of field-scale experiments (e.g., Higgins, Meneveau and Parlange, 2009; Kelly, Wyngaard and Sullivan, 2009; Bou-Zeid *et al.*, 2010; Patton *et al.*, 2011). However, the main drawback of the similarity theory is that it only holds for idealized stationary conditions, which are rarely met in practice, resulting in a model containing strong assumptions, which often leads to significant errors (Ha *et al.*, 2007; Higgins *et al.*, 2012; Thomas *et al.*, 2012). In real, non-idealized situations (such as field experiments), even slight surface heterogeneities can lead to dramatic impacts on the spatial structure of the flow in the surface boundary layer. I.e., in complex terrains, like forests, using Taylor's hypothesis is not possible. Even if perfect surface homogeneity was possible, other atmospheric (surface) conditions are often nonstationary as well (Holtslag *et al.*, 2013).

High resolution measurement could be used to check how good/bad the assumptions made are and would perhaps reduce the need for such assumptions in real-world cases. In the past decade, a way to obtain spatial distributed measurements is introduced into environmental studies. Distributed Temperature Sensing (DTS) technology measures temperature at high temporal and spatial resolution over distances of up to several kilometers by using Fiber Optic (FO) cables as sensors (Selker *et al.*, 2006a, 2006b; Tyler *et al.*, 2009). High-end DTS can measure the temperature at a 1 s and 0.3 m resolution (Sayde *et al.*, 2014). The ability to report temperature at such high resolution has proven useful in many environmental studies (Selker *et al.*, 2006a, 2006b; Tyler *et al.*, 2008, 2009; Steele-Dunne *et al.*, 2010), including atmospheric experiments (Keller *et al.*, 2011; Petrides *et al.*, 2011; Schilperoort *et al.*, 2018). It has also been shown that it is possible to observe air temperature and thermal structure of near-surface turbulence with DTS (Thomas *et al.*, 2012; Euser *et al.*, 2014; Zeeman, Selker and Thomas, 2015).

Recently, Sayde *et al.* (2015), introduced the AHFO technique as a means of performing independent explicit wind speed measurements using distributed temperature sensing (DTS) technology. The underlying concept of the proposed method is similar to that of a hotwire anemometer; however, instead of single point measurements, AFHO enables multiple measurements to be made at very high spatial resolution. AHFO has the potential to capture turbulent motions, providing significant insight into (turbulent) atmospheric surface layer flows. Instead of only passively measuring the temperature in the fiber (as is done with DTS), one segment of the cable is actively heated. By positioning parallel heated and reference segments of the fiber close to each other (i.e., in the order of 0.1 m), it is possible to measure the temperature difference between the heated and reference fiber, i.e., the heated fiber and the air temperature. The temperature difference between the cables depends on the energy input as well as on the wind speed of the ambient air, which determines the magnitude of the lateral heat exchange, through advection of cooler ambient air. By setting up an energy balance for the heated cable, one can estimate the magnitude of this advective heat transport. Finally, from this an estimate of the wind speed is made.

Results from a field study by Sayde et al. (2015) demonstrated promising performance of the AHFO technique; however, they recommended further tests be performed in controlled airflow conditions. First, the heat transfer model assumes the flow is normal to the axis of the fiber. Sayde et al. (2015) developed a first-order estimate of the influence of a non-normal angle of attack (the difference between the wind direction and the axis of the fiber), using a directional sensitivity equation from hotwire anemometry (Webster, 1962; Hinze, 1975; Perry, 1982; Adrian *et al.*, 1984), but it needs to be tested in a controlled setting to determine its validity. Second, Sayde et al. (2015) highlight the importance of a sufficient signal-to-noise ratio when conducting measurements. They show that the temperature difference between the heated and reference segments gives a good estimate for this ratio. The influence of these two topics on the measurement accuracy and precision is investigated and the results are used to propose a method to estimate the precision for future experiments with AHFO, hence our work will improve the possibilities for successful application of AHFO in future field experiments.

An overview of the experimental setup is presented in section 2, with the accuracy and precision of the AHFO experiments presented in chapter 3. In section 4, the method for estimating the precision for future experiments is introduced, followed by a short note on future studies.

2. Experimental Set-Up and Methods

2.1 Wind tunnel experiments

To study the directional sensitivity and influence of the signal-to-noise ratio we conducted a series of experiments under tightly controlled airflow conditions to improve the applicability of AHFO in experimental (field) research. The experiments presented were performed in a wind tunnel at Oregon State University. This wind tunnel has a closed circuit, which means the air inside is recycled. At the test section the wind tunnel has a cross-section (height by width) of 1.23 by 1.52 m and an undisturbed horizontal section of roughly 5 to 6 m which may be used for probing. During the experiment two segments of one cable (which encloses the FO's) were placed 8 cm apart: one heated and one reference segment. For validation, an independent sonic anemometer was placed closely (approximately 0.2 m) behind the fibers, which measures the wind speed in 3 directions. All equipment was mounted using custom-designed support material.

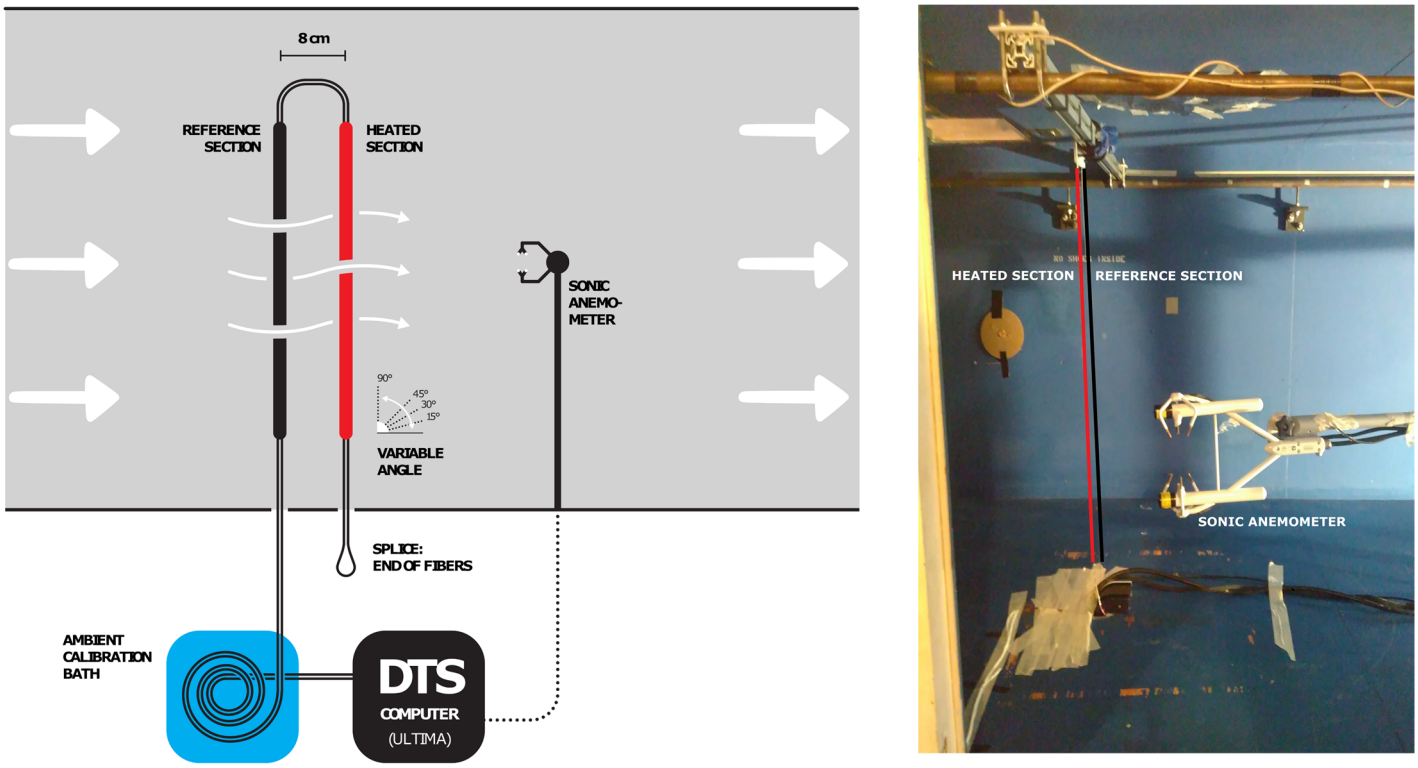

Figure 1 a) Schematic of the wind tunnel setup and b) photograph of the experimental setup in the wind tunnel.

During the experiment, the angle, wind speed and heating rate were changed step-by-step in a systematic manner. To create the temperature difference (ΔT, e.g., 2 °C) needed to determine wind speed, a constant electrical current (I) is passed through the heated cable. By fixing the current through the stainless steel casing of the cable, the entire FO cable is heated because of the electrical resistance (R) of the stainless steel casing. The magnitude of the current needed to create a given temperature difference is dependent on the cable resistance and the wind speed, therefore the current is changed for each individual experiment. The amount of power applied per meter of cable, P_s (Wm^{-1}), necessary to heat the cable and to create a temperature difference, is referred to as the heating rate. The AFHO wind speed measurements can be calibrated by comparing the AFHO wind speed to a reference sonic anemometer. The wind speed in the wind tunnel was fixed at a constant value to create a steady state flow; however in field experiments the wind speed will vary, the temperature difference will fluctuate accordingly if the current is fixed.

The cable was mounted at four different angles in the wind tunnel, resulting in different angles of attack, in order to gain more insights into directional sensitivity. In Figure 1b the 90° set-up is visible, however the cable was also mounted at a 45°, 30° and 15° angle, with respect to the floor of the wind tunnel (see: Figure 1a, inset). During all set-ups, the lower part was always fixed to the opening in the bottom of the wind tunnel, while the upper end was attached to an extruded aluminum bar that was moved over the fixed horizontal bars, to achieve the desired cable angles. To test the performance for a range of wind speeds, ten different wind speeds were tested for every angle: 1, 3, 5, 7, 9, 11, 13, 15, 16 and 17 ms^{-1} (e.g., 4x10 = 40 setups). Finally for all angles and every wind speed, three temperature differences were applied in order to quantify the importance of the signal-to-noise ratio. The current was fixed to create a temperature difference (ΔT) of 2, 4 and 6 °C between the heated and reference cable. In total, 120 (4 x 10 x 3) small experiments were conducted with the different parameters, each with a minimum duration of 10 minutes.

The cable mounted in the wind tunnel consisted of a 1.34 mm outer diameter stainless steel casing that enclosed four multi-mode FO's with a diameter of 62.5 µm (Figure 2). Only two FO's were used and these were spliced at the end of the cable to create a duplexed FO, which results in double measurements (Hausner *et al.*, 2011). The FO's were connected to a Silixa Ultima DTS machine (Ultima S, 2 km range, Silixa, London, UK) outside the wind tunnel.

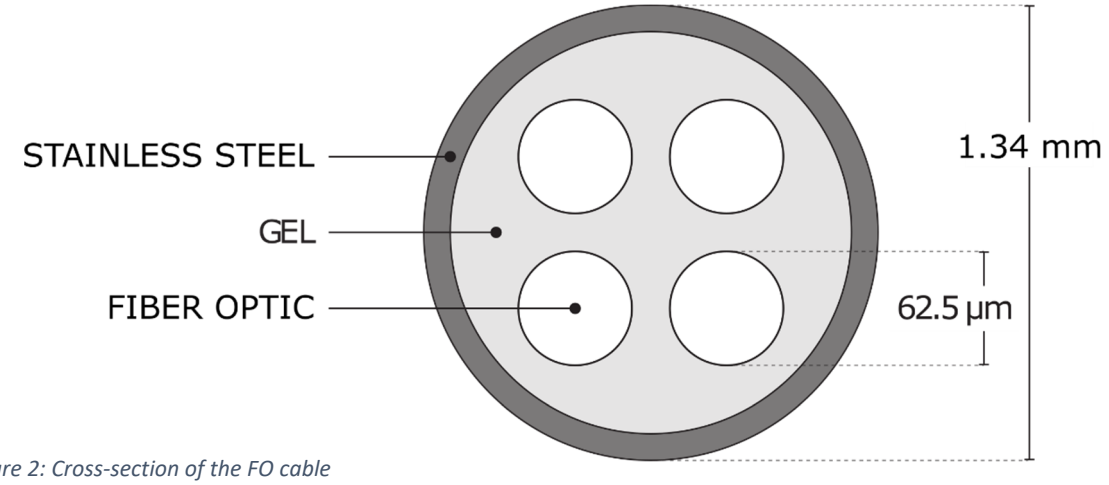

Figure 2: Cross-section of the FO cable

As the cable was looped through the wind tunnel, one cable segment was heated. To heat the cable in a controlled way, the stainless steel casing was connected to a power controller (MicroFUSION uF1HXTA0-32-P1000-F040) by 12 AWG cables (3.31 mm^2). Different heating rates varying from 0.5-10 Wm^{-1} were used to create temperature differences to a fixed level, either 2, 4 and 6 °C depending on the setup. The electrical resistance per meter of stainless steel casing (R_s) is 1.67 (Ωm^{-1}) and is constant along the length. For the length of a cable segment (B, (m)), $R = R_s B$, where R (Ω) is the total resistance of a cable segment. The same holds for $P = P_s B$, where P (W) is the total power input for a cable segment. The heating rate for a cable segment (Wm^{-1}) was controlled by fixing the current, I (A), during experiments, as the current is also constant over the entire heated segment, the heating rate is as well. Hence, the known relation $P = I^2 R$ (W), or in this specific case the heating rate is $P_s = I^2 R_s$ (Wm^{-1}) per meter of cable segment.

For calibration and validation of the DTS data, approximately 6 m of the FO cables was placed in a well-mixed ambient to calibrate the DTS temperature according to the method described by Hausner *et al.*, 2011. The temperature was verified with one probe (RBRsolo^2 T, RBR Ltd., Ottawa, Ontario, Canada). A circulating aquarium pump was placed inside the bath, to prevent stratification.

Temperatures along the FO's were sampled at 0.125 m resolution with a sampling rate of 1 Hz. The FO's were deployed in a double-ended configuration, however the data was acquired and treated as two separated single-ended channels of data. Splices between ends of fiber optic cables are known to create an additional loss in signal, i.e., local higher attenuation (Tyler *et al.*, 2009; van de Giesen *et al.*, 2012), this loss is normally independent of the direction. However, in processing of the raw DTS data it was found that the loss over the splice was not the same in both directions. Due to this asymmetrical structure of the splice loss, only the data of one channel was used in order to ensure the quality of the results, as this channel showed a regular splice loss.

To be able to test the accuracy of the DTS wind speed measurements independently, wind speed was sampled at 10 Hz using a sonic anemometer, including a gasometer and logger (IRGASON+EC100 and CR3000, Campbell Scientific, Logan, UT,USA). The sonic anemometer was mounted approximately 0.2 m behind the fiber optics, in the middle of the wind tunnel. As the FO's are very thin it is assumed that these do not significantly disturb the measurement of the sonic volume (particularly at larger averaging times). However, in reality some disturbance will always be present.

2.2 Determination of Wind Speed

2.2.1 Determination of the Wind Speed

An energy balance is used to quantify the advective energy transport from the heated cable, and therefore estimate the wind speed with DTS. The advective cooling can be converted to wind speed, because it is a function of wind speed and the temperature difference between the heated and unheated segments. The full energy balance (in W) for a cable segment volume is given by Sayde et al. (2015), and schematically shown in Figure 3:

$$c_s \rho_v V \frac{\mathrm{d}T_s}{\mathrm{d}t} = P_s B + (\bar{S}_b + \bar{S}_d + \alpha_s \bar{S}_t)(1 - \alpha_f) 2r\pi B + (\bar{L}_\downarrow + \bar{L}_\uparrow)\varepsilon 2r\pi B - \varepsilon\sigma T_s^4 2r\pi B - h(T_s - T_f) 2r\pi B \quad (1)$$

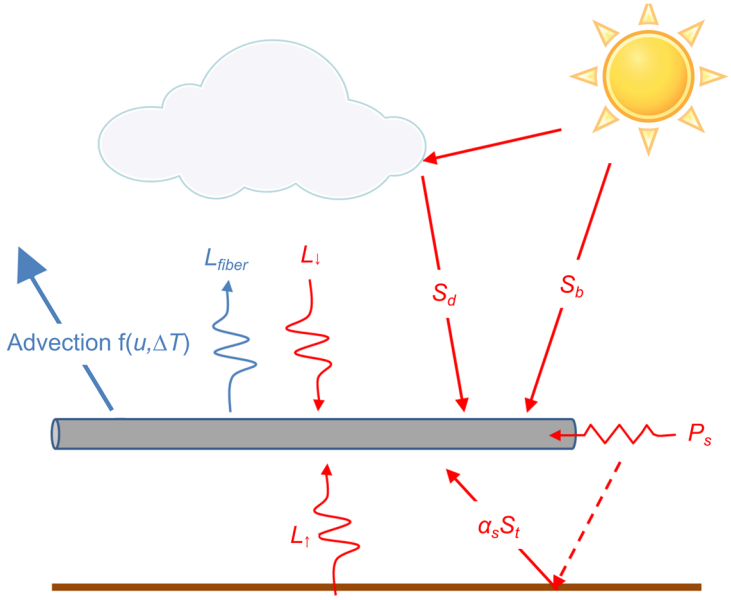

Figure 3: Schematization of the energy balance, based on Sayde et al. (2015)

Where, *r* is the radius of the cable, 6.7 x 10^{-4} m in our setup; *V* is the volume of the cable segment ($\pi r^2 B$, in m^3), c_s is the specific heat capacity of the FO cable (502 $\mathrm{Jkg^{-1}K^{-1}}$) and ρ_v is the FO cable density: 800 $\mathrm{kgm^{-3}}$. P_s is the heating rate per meter of cable (in $\mathrm{Wm^{-1}}$); and *B* is the length of a cable segment (in m). $\bar{S}_b, \bar{S}_d$ and $\alpha_s \bar{S}_t$ (in $\mathrm{Wm^{-2}}$) are the mean direct, diffuse and reflected short wave radiation fluxes, respectively, with α_s being the surface albedo of the ground; and α_f is the FO cable optic surface albedo. $\bar{L}_{\downarrow} + \bar{L}_{\uparrow}$ (in $\mathrm{Wm^{-2}}$) are the average downward and upward longwave radiation fluxes, respectively; and ε is the FO cable surface emissivity. Based on the kind of stainless steel, emissivity values can range from 0.3 to 0.7 (Baldwin and Lovell-Smith, 1992); however, we assume a value of 0.5 (Madhusudana, 2000). σ is the Stefan-Boltzmann constant, 5.67 x 10^{-8} ($\mathrm{Wm^{-2}K^{-4}}$); and $\varepsilon\sigma T_s^4$ is the outgoing longwave radiation of the fiber, i.e., L_{fiber}; T_s and T_f are the temperature (in K) of the heated cable segment and (unheated) reference segment (i.e., air temperature), respectively. Finally, *h* is the advective heat transfer coefficient (in $\mathrm{Js^{-1}m^{-2}K^{-1}}$). By means of the dimensionless Nusselt (Nu), Prandtl (Pr), and Reynolds (Re) numbers, *h* can be expressed as function of the wind speed, $h = f(u_n)$. Nu, is the ratio between the advective and conductive heat transfer, where the Nusselt number can be written as follows, (Žukauskas, 1972):

$$\mathrm{Nu} = \frac{h\, d_s}{K_a} \quad (2),$$

with,

$$\mathrm{Nu} = C\mathrm{Re}^m \mathrm{Pr}^n \left(\frac{\mathrm{Pr}}{\mathrm{Pr}_s}\right)^{\frac{1}{4}} \quad (3)$$

$$\mathrm{Re} = \frac{u_n d_s}{\upsilon_a} \quad (4)$$

d_s is the fibers characteristic length (2*r*); K_a is the thermal conductivity of air and υ_a the kinematic viscosity of air, respectively 0.0255 $\mathrm{Js^{-1}m^{-1}K^{-1}}$and 1.5 x 10^{-5} $\mathrm{m^2s^{-1}}$(Tsilingiris, 2008). $K_a$and $\upsilon_a$are assumed to be constant, due to the controlled conditions in the wind tunnel, but in field experiments this should be included as a variable, as $K_a$and υ_a are temperature and relative humidity depend (Tsilingiris, 2008). *C*, *m* and *n* are empirical constants related to forced advection of heat by air movement. In Sayde et al. (2015), *C*, *m* and *n* values of 0.51, 0.5 and 0.37 are set, based on (Žukauskas, 1972). Pr is the Prandtl number and can be seen as the ratio between kinematic viscosity and thermal diffusivity, which, we assume to be constant (0.72) for our range of temperatures (12-35 °C), as in Tsilingiris, (2008). Pr_s is the Prandtl number for the temperature of the heated fiber segment, which is assumed to be the same as Pr, due to the small temperature differences (max 6 °C). Lastly, Re is the Reynolds number which is used to determine the flow regime of the air along the fiber segments, i.e., Re expresses if the flow regime is laminar or turbulent. Eq. 2-4, *h* can be expressed as:

$$h = C(d)^{m-1}\mathrm{Pr}^n \left(\frac{\mathrm{Pr}}{\mathrm{Pr}_s}\right)^{\frac{1}{4}} K_a {\upsilon_a}^{-m} {u_n}^m \quad (5)$$

Consequently, the determination of the Nusselt number (Eq. 3) is only valid in the following ranges of Re (40-1000) and Pr (0.7-500). Where Re can be a limitation for higher wind speeds, especially when the diameter of the fiber is large, in our case wind speeds higher than approximately 11 $\mathrm{ms^{-1}}$ would be out of range. In the derivation of the energy balance (Eq. 1), There is assumed to be no free convection, induced by heating of the air close to the cable, and no conduction of heat in the axial direction of the FO cable. It is also assumed there is no radiative exchange between objects

close and parallel to the heated fiber, i.e., dispersion of heat from the heated cable to the reference cable is assumed to be negligible. Furthermore, a flow directed normal to the axis of FO cable is assumed by the proposed energy balance, i.e., for flow directed in a different angle, compensation is necessary in order to accurately estimate the wind speed.

Finally, the energy balance is simplified, by dividing Eq. 1 by $2r\pi B$, which is equal to the surface area of the FO cable. The energy balance now no longer depends on B, meaning the length of FO segment does not need to be defined. The proposed final energy balance by Sayde et al. (2015) is as follows and in Wm^{-2}:

$$\frac{c_s \rho r}{2}\frac{\mathrm{d}T_s}{\mathrm{d}t} = \frac{P_s}{2\pi r} + (\bar{S}_b + \bar{S}_d + \rho\bar{S}_t)(1-\alpha) + (\bar{L}_\downarrow + \bar{L}_\uparrow)\varepsilon - \varepsilon\sigma T_s^4 - h\left(T_s - T_f\right) \quad (6)$$

where, ρ is the FO cable density per meter of cable segment: 4.5 x 10^{-3} kgm^{-1}.

2.2.2. Proposed simplified determination of the Wind Speed

Due to the setup inside the wind tunnel, as opposed to outdoor conditions, some simplifications can be made. The short wave radiation can be neglected because it is an indoor experiment (no sunlight). Furthermore, we assume that there is a uniform temperature inside the wind tunnel, due to the enclosed conditions. This means the incoming radiation is dependent on the air temperature, T_f. Assuming incoming $(\bar{L}_\downarrow + \bar{L}_\uparrow)$ to be black body radiation (i.e., $L_{in} = \sigma T_s^4$), the net longwave radiation loss for the fiber can be simplified accordingly by merging the incoming longwave and outgoing longwave radiation as:

$$(\bar{L}_\downarrow + \bar{L}_\uparrow)\varepsilon - \varepsilon\sigma T_s^4 \approx -\varepsilon\sigma\left(T_s^4 - T_f^4\right) \quad (7)$$

One more additional change is made, based on our results obtained during testing of the performance of the AHFO technique. In processing of the obtained wind tunnel data it was found that by using the calculation of the Nusselt number from Žukauskas (1972), Eq. 2 , a ~20 % additional bias in calculating the wind speed was created. By using a more recent version for calculating the empirical Nusselt number (Cengel and Ghajar, 2014), the bias in our study is reduced to ~5 %. Therefore, Eq. 8 is proposed to calculate the Nusselt number, where the constants *C*, *m* and *n* are still used; however, with the values from Table 7-1 (*C* = 0.683, *m* = 0.466 and *n* =1/3) in Cengel and Ghajar, (2014), rather than those in Žukauskas (1972). Next to the improved fit, the range of Re over which the equation is valid is much wider (40-4000 compared with 40-1000), and therefore more applicable in future AHFO experiments.

$$\mathrm{Nu} = C\mathrm{Re}^m\mathrm{Pr}^n = 0.683\mathrm{Re}^{0.46}\mathrm{Pr}^{\frac{1}{3}} \quad (8)$$

Consequently, the expression of *h* changes as well.

$$h = C(d)^{m-1}\mathrm{Pr}^n K_a {v_a}^{-m} {u_n}^m \quad (9)$$

Taking the long and short wave radiation simplifications and using a different way to calculate the advective heat transfer coefficient (*h*) into account, the energy balance can be simplified as follow.

$$\frac{c_s \rho r}{2}\frac{\mathrm{d}T_s}{\mathrm{d}t} = \frac{P_s}{2\pi r} - \varepsilon\sigma\left(T_s^4 - T_f^4\right) - h\left(T_s - T_f\right) \quad (10)$$

By substituting the expression for *h* (Eq. 9), we can rearrange Eq. 10 to obtain an expression for wind speed. Eq. 11 will be used to estimate the wind speed in our wind tunnel study.

$$u_N = \left(\frac{0.5\ P\ \pi^{-1} r^{-1} - \varepsilon\sigma\left(T_s^4 - T_f^4\right) - \frac{1}{2} c_p \rho r \frac{\mathrm{d}T_s}{\mathrm{d}t}}{C(2r)^{m-1} \mathrm{Pr}^n K_a v_a^{-m} (T_s - T_f)} \right)^{\frac{1}{m}} \quad (11)$$

2.3 Directional Sensitivity analysis

Equation 11 is derived for flows normal to axis of the cable (as in Figure 1b). However, in reality the wind will not always have a 90° angle compared to the axis of the cable, especially in outside atmospheric experiments. For angles smaller than 90° the wind speed will be underestimated, as the advective heat transfer is less efficient. To be able to still determine the wind speed for all angles of attack, Sayde et al. (2015) adjust the wind speed obtained in Eq. 11 using a geometric correction from hotwire anemometry (e.g., Adrian et al., 1984) to get the true wind speed (u_{DTS}):

$$u_{DTS} = \sqrt{\frac{{u_N}^2}{[\cos^2(\varphi - 90°) + k^2 \sin^2(\varphi - 90°)]}} \quad (12)$$

k is the directional sensitivity and φ is the angle of attack of the wind with respect to the axis of the cable, ranging from 0° to 90°.

However, during analysis of the wind tunnel data it was found that Eq. 12 was not giving satisfying results (e.g., a 22 % bias between the 90° and 15° angle). In Adrian *et al.*, (1984) is shown that in hotwire anemometry a variety of theoretical and empirical formulas are proposed in the past, in order to account for directional sensitivity. Alternatively, using the formula suggested by Bruun, (1971) gives more satisfying results, diminishing the bias between the 90° and 15° angle to only 5 %.

$$u_{DTS} = \frac{u_N}{\cos(\varphi - 90°)^{m_1}} \quad (13)$$

Therefore, Eq. 13 is used to account for directional sensitivity in our study, with the scaling exponent, m_1, able to be optimized during calibration of the AHFO measurements. The value for m_1 obtained during calibration of our set up was 1.05.

2.4 DTS and Signal-to-Noise ratio analysis

Based on the backscattered signal of a laser pulse inside fiber optic cables, a Distributed Temperature Sensing (DTS) machine measures temperature along a complete fiber optic cable (Selker *et al.*, 2006b). This fiber optic cables can have lengths up to several kilometers with a spatial resolution up to 0.3 m, i.e., one DTS machine leads to thousands of individual measurements. Laser pulses are sent with a fixed wavelength and most backscattered light keeps this wavelength, however some backscattered laser shifts to a shorter or longer wavelength, these frequency-shifted reflection are referred to as Raman-backscatter (Selker *et al.*, 2006a). By counting the backscattered photons with a longer (Stokes) and shorter (Anti-Stokes) frequency, a ratio between these two can be calculated. The strength of the Anti-Stokes signal is depended on temperature, hence the ratio between the power of the Stokes and Anti-Stokes changes with temperature; this principle is used to measure the temperature along the cable. Consequently, a main source of noise in DTS data is: white noise induced by the statistical variability in photon count from backscatter (optical shot noise), which is important for further data quality analysis and is also influencing the signal-to-noise

ratio. Besides, other sources of noise exist as well (e.g. Johnson-Nyquist noise), which can be taken into consideration.

A sufficiently high signal-to-noise ratio is essential for measurement precision with DTS. In Sayde et al. (2015) is shown, the signal-to-noise ratio can be described as: $(T_s - T_f)/\sigma_T$. Hence the signal-to-noise ratio is related to the ΔT ($T_s - T_f$) and the measurement error of the DTS, σ_T (in this study at a 1 s sample resolution), and can be assumed constant in a lab experiment. A large ΔT is obviously desirable, however, due to limitations ΔT cannot be increased infinitely; e.g., the power controller can only deliver a limited amount of power to heat the fiber, which is especially relevant for the heating of long lengths of FO cable (i.e. several hundreds of meters of FO cable), also the creation of larger temperature differences means the importance of other modes of energy transfer changes. In order to find realistic solutions, the effect of ΔT is investigated, therefore three temperature differences are created during the experiment. The effect of the signal-to-noise ratio is quantified, and an equation to estimate the precision is presented. The precision is an indication of the variability of wind speed (e.g., RMSD), as opposed to accuracy which describes a systematic measurement error that can be removed through calibration (e.g., a bias).

3. Results

The accuracy and precision of the DTS wind speed calculations is given in Figure 4 and 5, where the velocity calculated using AHFO (calculated by Eq. 11 and 13) is compared with the velocity measured with the sonic anemometer. The temperatures measured with AHFO are spatially averaged over 10 measurements (2 fibers of each 5 measurements), i.e., this is equivalent to a height of ~0.9 m in the wind tunnel. Only the temperatures from in the middle of the wind tunnel are used, to prevent using data with side/boundary effects. Figure 4 shows the 1 s sample rate DTS data against the 1 s average sonic anemometer data, for the four different angles of attack. Figure 5 shows the same dataset, but temporally averaged over 30 s, and for all angles. A clear improvement of the precision is visible when temporal averaging is performed. Even though the directional sensitivity formula is not yet fully calibrated, the bias is negligible, with a coefficients of determination of ranging from 0.94-0.99. Finally, as expected, the wind speed measurement are less accurate when the wind speed angle is smaller.

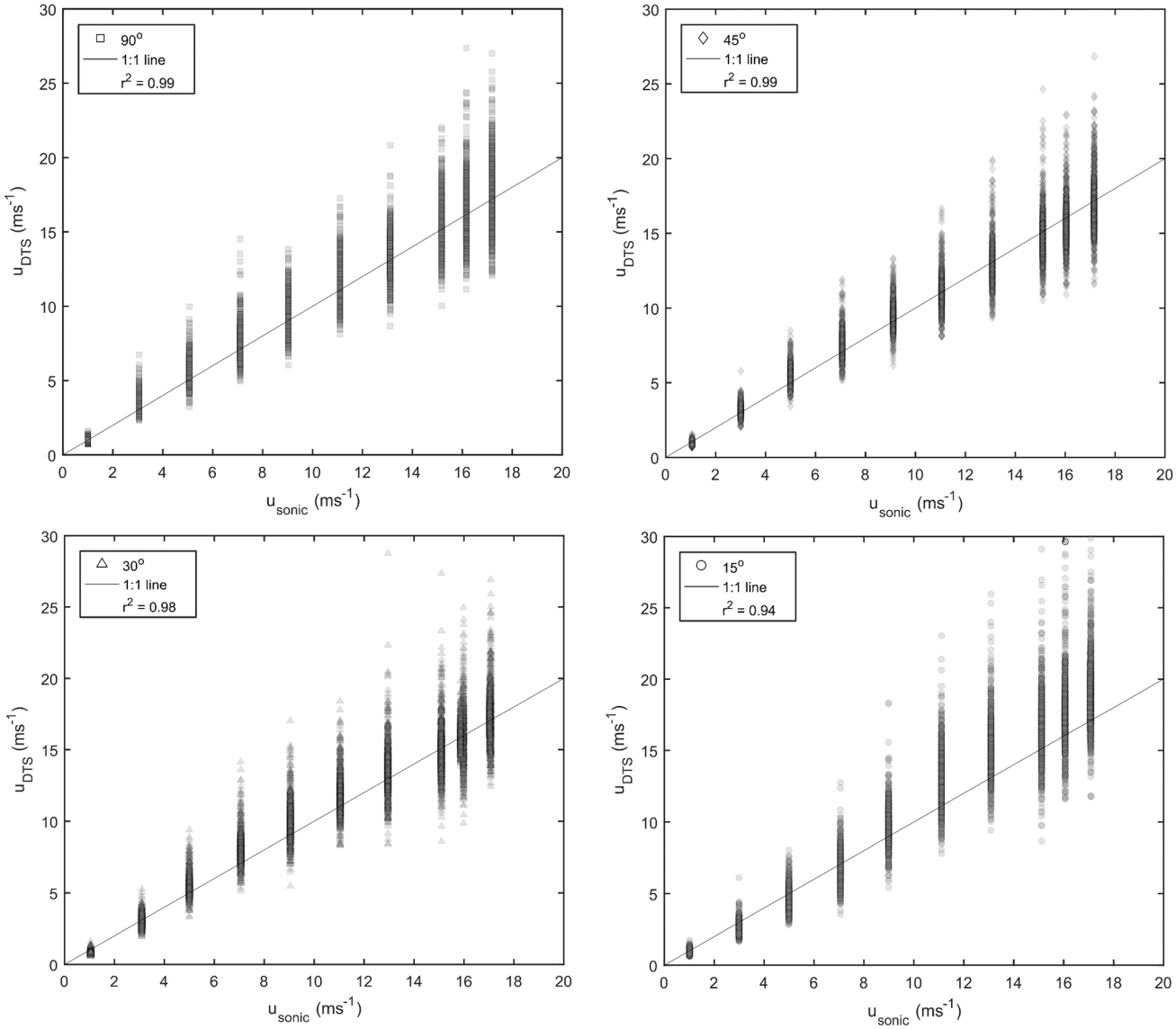

Figure 4a-d: Comparison of AHFO and sonic anemometer wind speed at a 1 s temporal resolution, for the four different angles of attack: a) 90°, b) 45°, c) 30°, and d) 15°.

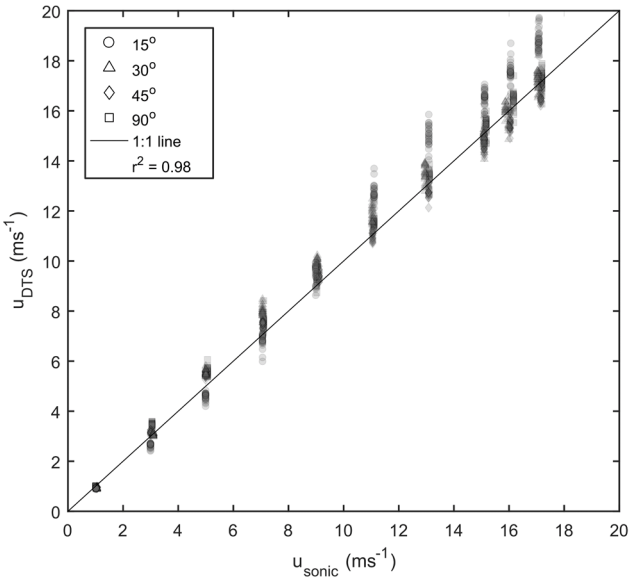

Figure 5: Comparison of AHFO and sonic anemometer wind speed averaged over 30 s for all angles of attack.

To get more insight in the quality of the results, a dimensionless analysis is performed. In Figure 6, the non-dimensional wind speed accuracy for the whole wind tunnel experiment is shown. For all combinations (120 individual cases of varying wind speed, angle and ΔT), the accuracy is calculated according to Eq. 14. The accuracy is then averaged over wind speed for each ΔT and angle combination in Figure 6, indicating the size of the bias by σ_a.

$$\sigma_a = \frac{\bar{u}_{DTS} - \bar{u}_{sonic}}{\bar{u}_{sonic}} \quad (14)$$

For the whole uncalibrated data set, the maximum σ_a is 5 %, which is promising for future applications. The 90° angle should be the best performing angle, however it is overestimating with 5 %, which is probably due to neglecting of small energy losses, like free convection, due to heating of air close to the heated cable, creating local convection of lighter/warmer air (Sayde *et al.*, 2015). When such an energy losses would be implemented it will affect all angles, hence the bias of each angle will change. As a flow directed normal to the axis of FO cable is assumed by the proposed energy balance, it is better to compare the other angles to the 90° angle instead of 0 bias. Doing this, it can been seen that the directional sensitivity formula is not yet optimally calibrated (e.g., the 5 % difference between the 90° and 15° angle biases). This kind of error is not uncommon and in accordance with previous hotwire anemometry work, especially with small angles of attack (Adrian *et al.*, 1984). Nevertheless, the bias is fairly constant with increasing averaging time, which means extensive calibration can probably increase the accuracy.

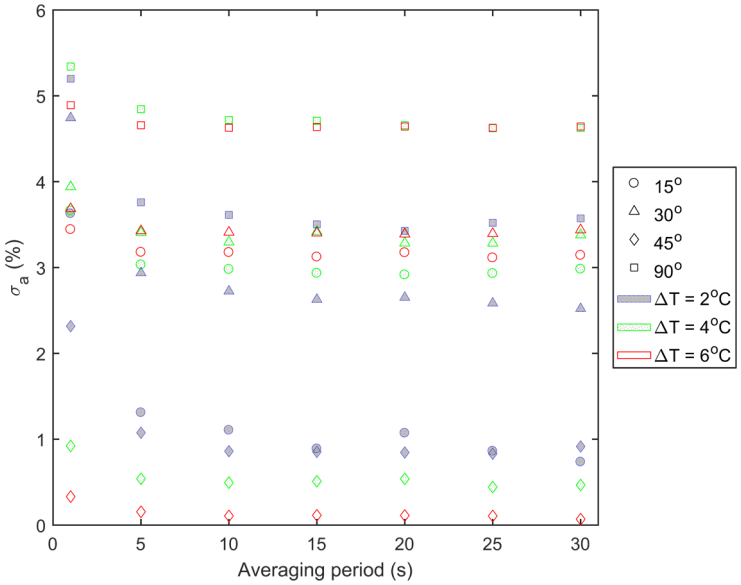

Figure 6: Bias in AHFO wind speed as a function of averaging period for different angles of attack, and different fiber heating.

While the accuracy (bias) remains constant over averaging period, the relative precision, σ_p decreases significantly (Fig 7). The precision is calculated for all 120 ΔT, angle and wind speed combination, using Eq. 15. To be able to present the precision clearly, the precision is averaged over wind speed for all ΔT and angle combinations in Figure 7:

$$\sigma_p = \frac{\mathrm{RMSD}}{\bar{u}} = \frac{\sqrt{\frac{\sum((u_{sonic}(i) - \bar{u}_{sonic}) - (u_{DTS}(i) - \bar{u}_{DTS}))^2}{n}}}{\bar{u}_{sonic}} \quad (15)$$

While calculating the precision of u_{DTS}, the natural variability of the wind is excluded, by assuming the sonic anemometer is able to capture this. As a results the variability of the DTS machine u_{DTS} estimates are obtained. For each of the 120 combinations, $\bar{u}_{sonic}$ and $\bar{u}_{DTS}$ are the average wind speeds for a combination. $u_{sonic}(i)$ and $u_{DTS}(i)$ are single measurements during this combination.

The precision increases to a σ_p less than 5 % by averaging over time. Improvement by averaging is expected due to the reduction of noise (van de Giesen *et al.*, 2012). As mentioned, the main source of noise in DTS data is white noise, this explains the visible improvement of the precision by $\frac{1}{\sqrt{n}}$, as signal averaging is applied, where *n* is the amount of measurements (Selker *et al.*, 2006b; Kaiser and Knight, 1979).

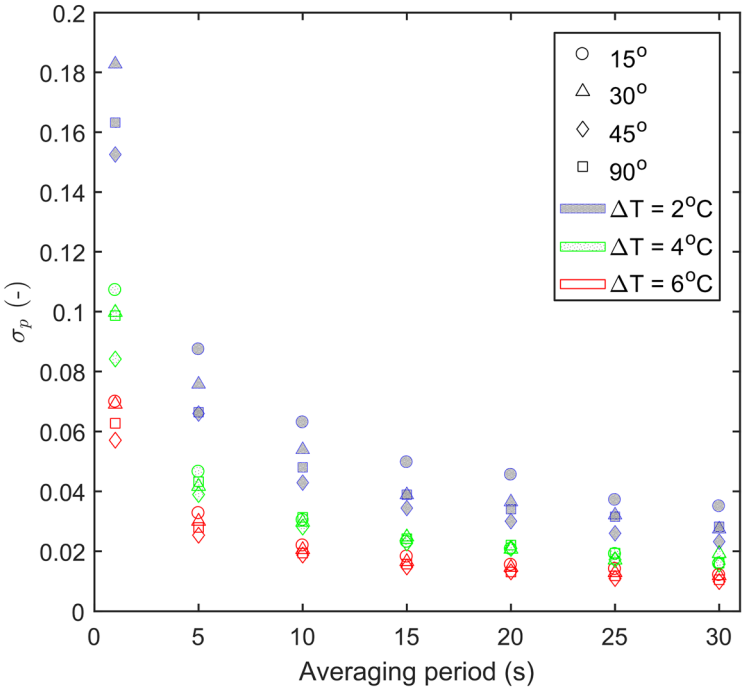

Figure 7: Precision of the AHFO wind speed measurements as a function of averaging period.

4. Discussion

4.1 Normalized precision

By normalizing it can be possible to find trends or behavior which are independent of arbitrary chosen settings like ΔT. Therefore, it is tried to normalize the precision in order to find useful independent behavior, which can be used to predict the precision for future experiments. First, the precision is normalized to ΔT (Figure 8a), by multiplying by $\frac{\Delta T}{T_{error}}$, the expected trend of $\frac{1}{\sqrt{n}}$ becomes even more clear, as shown by the black solid line showing $\frac{\gamma}{\sqrt{n}}$, where γ is σ_p at a 1 s temporal, and 10 measurement spatial, resolution. Secondly, the precision is also normalized to the $\frac{1}{\sqrt{n}}$ behavior, by multiplying by $\sqrt{\frac{t_{avg}}{t_{sample}}}$. It appears that the precision can be condensed in a number, 1.6, which we denote by the symbol C_{int} (Figure 8b). Intermediate constant C_{int} can be defined as, Eq. 16:

$$C_{int} = \gamma \frac{\Delta T}{T_{error}} \sqrt{\frac{t_{avg}}{t_{sample}}} = 1.6 \ (16)$$

Where, T_{error} and t_{sample} are given constants which depend on the performance of the DTS, in this case $T_{error} = 0.25$ K and $t_{sample} = 1$ s, according to the factory specifications.

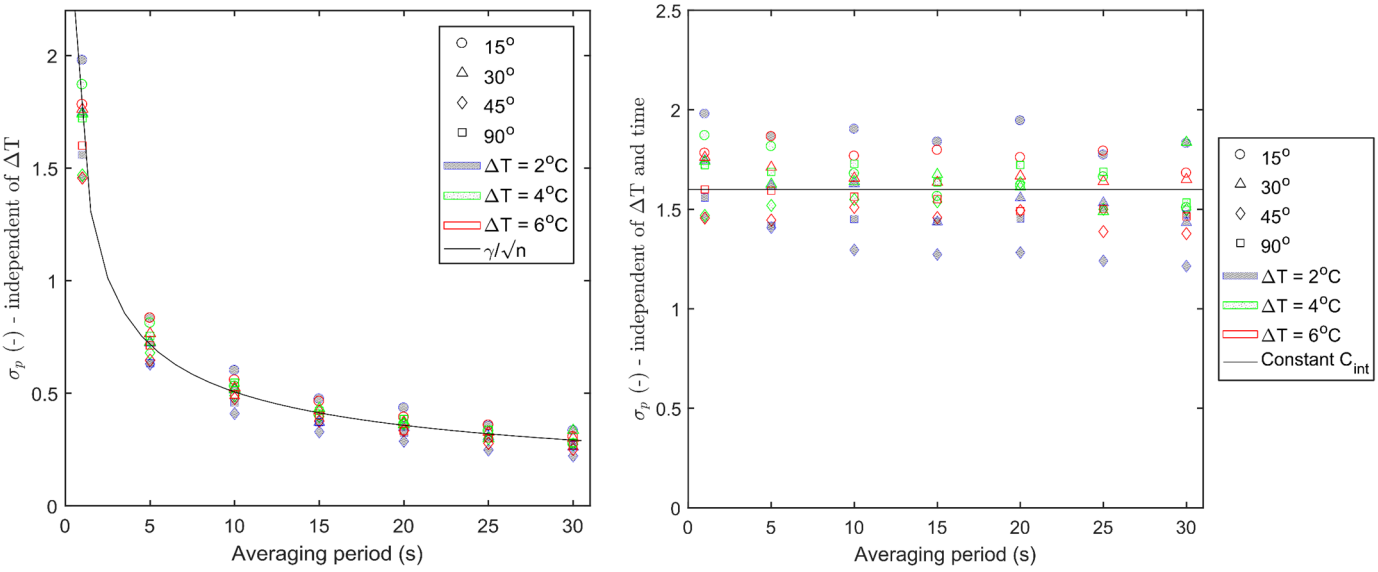

Figure 8 a) Precision of the AHFO wind speed measurements as a function of averaging period, independent of ΔT; and b) Precision of the AHFO wind speed measurements as a function of averaging period. Independent of ΔT and averaging period.

Finally, a final constant for a 1 s and 0.3 m resolution is desired, as this this is the starting point before any averaging takes place. Doing so, it is possible to increase the precision of the observation by either averaging over space or time, depending on the scientific research question to be answered with AHFO. By using the shown $\frac{1}{\sqrt{n}}$ dependency, we can easily convert C_{int} into C_{DTS}, by multiplying C_{int} by $\sqrt{\frac{10}{1}}$, as *n* is 10 times less.

$$C_{DTS} = C_{int}\sqrt{10} = 1.6\sqrt{10} = 5.06 \ (17)$$

4.2 Precision prediction

At the start of a new AHFO experiment it is unknown how to make sure the signal-to-noise ratio is sufficient, such that σ_p is small. However, given the shown result that the increase in precision behaves independent of *ΔT* and the averaging time, it is posible to make a prediction for the precision of future work.

In outdoor experiments, the only setting which can be changed is the heating rate, P_s, which is asssumed to be fixed at a single value. The idea behind the precision prediction is, to give an advise for a heating rate, such that a prevered precision is achieved for a known dominant wind speed range. As the wind speed outside will vary naturally, ΔT will change accordingly. Therefore, in order to obtain an expresion where P_s is the only unkown, ΔT first needs to be expressed as a funtion of the wind speed u_n and the heating rate (P_s). This can be done by using Eq. 11. In order to obtain a first estimate, some assumptions can be made. The numerator of Eq. 11 constists of three terms, of which the first one with heating rate (P_s) is dominant compared to the other ones, namely at 10-100 times bigger. When these minor terms are neglected Eq. 11 can be simplified to:

$$U_n = \left(\frac{0.5\, P_s\, \pi^{-1} r^{-1}}{C(2r)^{m-1} Pr^n K_a v_a^{-m} (T_s - T_f)} \right)^{\frac{1}{m}} = \left(\frac{A\, P_s}{B\, \Delta T} \right)^{\frac{1}{m}} \quad (18)$$

Where, $A = 0.5\, \pi^{-1} r^{-1}$, $B = C(2r)^{m-1} Pr^n K_a v_a^{-m}$ and $\Delta T = T_s - T_f$. Also, Eq. 18 can be rewritten into Eq. 19:

$$\Delta T = \frac{A\, P_s}{B\, {u_n}^m} \quad (19)$$

Knowing this expression of ΔT, Eq. 19 can again be rewritten into Eq. 20, which expresses the precision estimate, with P_s as only parameter which can be changed during an experiment.

$$\sigma_p = C_{DTS} \frac{B\, T_{error}\, {u_n}^m}{A\, P_s} \sqrt{\frac{1}{n}} \quad (20)$$

Where *n* is the amount of measurements over which is averaged, by averaging over either the space or time domain. By assuming that all constants are known from literature and the set-up, a first estimate of the error can be made for every velocity or heating rate given. If a dominant wind speed range for a new project is known, an associated heating rate can be found, so the error is sufficiently small.

As an example, here we show Figure 9, which gives an estimation based on the used 1 s and 0.675 m resolution. Furthermore, if the diameter of the fiber is different, this is taken into account via term *A* from Eq. 20, which includes the radius (*r*). Also, when a DTS machine with a different performance is used, this can be implemented by changing T_{error} accordingly. Of course different applications will prefer different space-time averaging windows, depending on the scientific research question to be answered with AHFO, this option is included by $\sqrt{\frac{1}{n}}$.

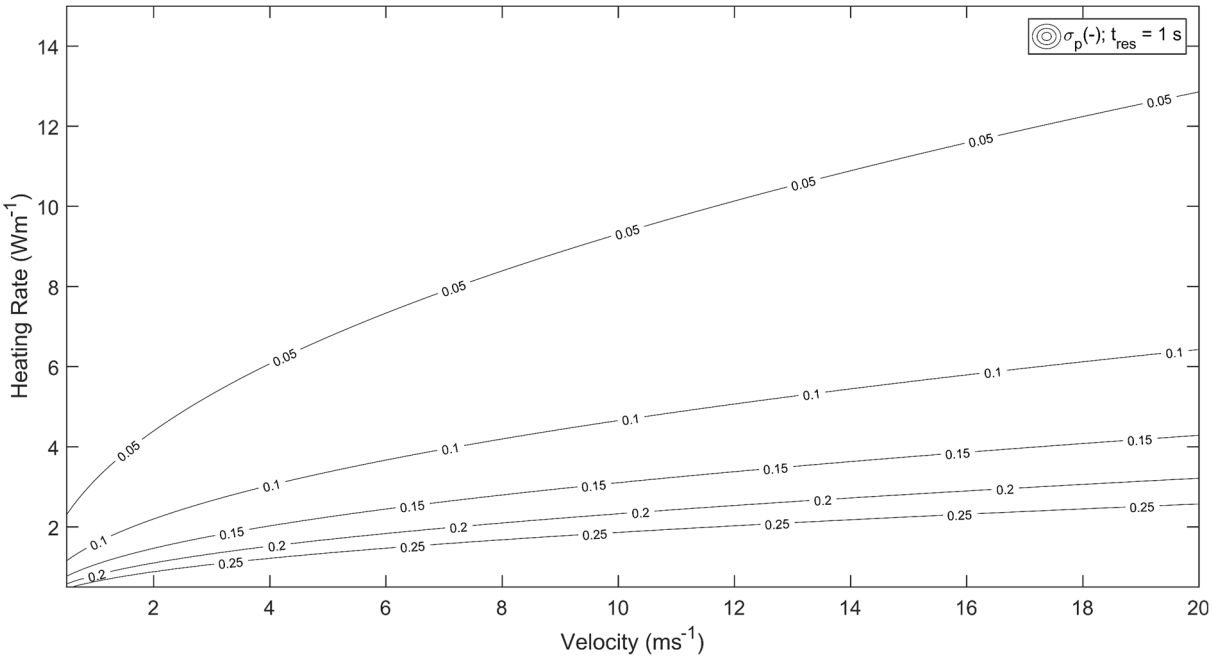

Figure 9: Expected error (contour lines) for a given heating rate and wind speed as calculated from Eq. 20, with a 1 s and 10 measurement resolution.

In outdoor experiments, the influence of the short and long wave radiation will be present. However, as long as the radiation is the same for the heated and non-heated segment, this does not influence the error estimation, as for the signal-to-noise ratio, ΔT is the most important factor. When the heated and reference fiber are close to each other, which is also needed for properly estimating the wind speed, both fibers will experience a similar contribution of external radiation, such that the overall ΔT will be relatively unaffected by this factor.

4.3 Using AHFO outdoors

The experiments described here were performed in a controlled wind tunnel environment. When performing outdoor AHFO experiments, several factors need to be considered. First of all, during field experiments the relative humidity and temperature might have such a big range that assuming certain parameters (e.g., $K_a$and υ_a) as constant is not applicable anymore (Tsilingiris, 2008). Furthermore, for small wind speeds (e.g., < 1 ms^{-1}), the neglection of energy losses like free convection seems not entirely applicable, as is visible in the strong convergence of the contour lines in Figure 9. This is confirmed in our study, where it was visible that the response is different between a well ventilated and non-ventilated cable, hence the accuracy is dependent on the wind speed. Although not shown in this paper, it seemed there was no time response difference between a vertical or horizontal mounted heated cable, however by mounting the cable in a horizontal or vertical direction, free convection might influence the temperature measurements as the heated air is moving upward. It is shown AHFO can give reliable wind speed measurements, however the precision and accuracy is not as good as with a sonic anemometer, the major addition of AHFO is the possibility to sample the wind speed with a high spatial distribution. Finally, when measuring in the field, the use of high quality reference point measurements (e.g., sonic anemometer) is recommended, for example to be able to compensate for possible biases. A sonic anemometer can also be useful to determine the angle of attack, as this is not (yet) possible with one single fiber, a more complex 3D set-up is necessary to be able to do this with DTS/AHFO (Zeeman, Selker and Thomas, 2015).

Despite the remarks, it will be interesting to perform outdoor tests in complex terrain, for both micrometeorological and hydrological applications, as AHFO gives a lot of insights in spatial varying wind fields. AHFO can be especially interesting in non-homogenous field sites, like forests, which are

already studied with other DTS applications (Schilperoort *et al.*, 2018). Also, it could be used to test the Taylor's frozen flow hypothesis, to estimate fluxes with the similarity theory. Moreover, the ability to measure spatial varying wind fields can be useful for estimating sensible heat fluxes in a variety of atmosphere-vegetation-soil continuums. Also, interesting work on measuring low wind speeds with Fiber Optics is recently published by Garcia-Ruiz *et al.*, (2018), which perhaps can be useful to in the future be able to measure wind speeds in a large range, including wind speeds smaller than 1 ms^{-1}.

5. Conclusions

Through a series of controlled wind tunnel experiments, new insights into the accuracy and precision of the newly introduced AHFO wind speed measuring technique were obtained. With high spatial (0.3 m) and temporal (1 s) resolution, the AHFO wind speed measurements agreed very well with the sonic anemometer measurements, with a coefficients of determination ranging from 0.94-0.99. It is also shown that the AHFO technique has the possibility to measure with a precision and accuracy of 95 %. Some additional work is possible, as there still is a small overall overestimation, which probably is caused by neglecting some energy fluxes, like free convection due to heating of the air close the heated cable. Furthermore, it is possible to optimize the directional sensitivity compensation by extended calibration.

The error prediction equation (Eq. 20) will aid in the design of future experiments. This design tool helps with choosing a heating rate for the heated fiber, to be able to create a sufficiently high signal-to-noise ratio. Based on the prevalent wind speeds of a potential field experiment site, a first estimate of an associated sufficient heating rate can be calculated. Due to the way this design tool is constructed, it can be used for all kinds of fibers, DTS precisions and user preferred spatial and temporal resolutions.

In this paper is shown that the AHFO technique can reliably measure wind speeds in a range of conditions. The combination of high spatial and temporal resolution with high precision of the technique opens a lot of possibilities in outdoor application, as the key feature of the AHFO is the ability to measure spatial structures in the flow, over scales ranging from one meter to several kilometers. In the future, the technique could be useful for micrometeorological and hydrological applications in complex terrain, allowing for characterization of spatial varying fields of mean wind speed, such as in canopy flows or in sloping terrain.

6. References

Adrian, R. J. *et al.* (1984) 'Aerodynamic disturbances of hot-wire probes and directional sensitivity', *Journal of Physics E: Scientific Instruments*, 17(1), pp. 62–71. doi: 10.1088/0022-3735/17/1/012.

Baldwin, A. J. and Lovell-Smith, J. E. R. (1992) 'The emissivity of stainless steel in dairy plant thermal design', *Journal of Food Engineering*, 17(4), pp. 281–289. doi: 10.1016/0260-8774(92)90045-8.

Bou-Zeid, E. *et al.* (2010) 'Field study of the dynamics and modelling of subgrid-scale turbulence in a stable atmospheric surface layer over a glacier', *Journal of Fluid Mechanics*, 665, pp. 480–515. doi: 10.1017/S0022112010004015.

Bruun, H. H. (1971) 'Interpretation of a Hot Wire Signal Using a Universal Calibration Law.', *Journal of Physics E: Scientific Instruments*, 4((MARCH, 1971)), pp. 225–231. doi: 10.1088/0022-3735/4/3/016.

Cengel, Y. and Ghajar, A. (2014) *Heat and mass transfer: fundamentals and applications*. McGraw-Hill Higher Education.

Euser, T. *et al.* (2014) 'A new method to measure Bowen ratios using high-resolution vertical dry and wet bulb temperature profiles', *Hydrology and Earth System Sciences*, 18(6), pp. 2021–2032. doi: 10.5194/hess-18-2021-2014.

Garcia-Ruiz, A. *et al.* (2018) 'Long-range distributed optical fiber hot-wire anemometer based on chirped-pulse ΦOTDR', *Optics Express*, 26(1), p. 463. doi: 10.1364/OE.26.000463.

van de Giesen, N. *et al.* (2012) 'Double-ended calibration of fiber-optic raman spectra distributed temperature sensing data', *Sensors (Switzerland)*, 12(5), pp. 5471–5485. doi: 10.3390/s120505471.

Goodberlet, M. A., Swift, C. T. and Wilkerson, J. C. (1989) 'Remote sensing of ocean surface winds with the special sensor microwave/imager', *Journal of Geophysical Research*, 94(C10), pp. 14547–14555. doi: 10.1029/JC094iC10p14547.

Ha, K.-J. *et al.* (2007) 'Evaluation of Boundary Layer Similarity Theory for Stable Conditions in CASES-99', *Monthly Weather Review*, 135(10), pp. 3474–3483. doi: 10.1175/MWR3488.1.

Hausner, M. B. *et al.* (2011) 'Calibrating single-ended fiber-optic raman spectra distributed temperature sensing data', *Sensors*, 11(11), pp. 10859–10879. doi: 10.3390/s111110859.

Higgins, C. W. *et al.* (2012) 'The Effect of Scale on the Applicability of Taylor's Frozen Turbulence Hypothesis in the Atmospheric Boundary Layer', *Boundary-Layer Meteorology*, 143(2), pp. 379–391. doi: 10.1007/s10546-012-9701-1.

Higgins, C. W., Meneveau, C. and Parlange, M. B. (2009) 'Geometric Alignments of the Subgrid-Scale Force in the Atmospheric Boundary Layer', *Boundary-Layer Meteorology*, 132(1), pp. 1–9. doi: 10.1007/s10546-009-9385-3.

Hinze, J. O. (1975) *Turbulence*. New York: McGraw-Hill Higher Education.

Holtslag, A. A. M. *et al.* (2013) 'Stable atmospheric boundary layers and diurnal cycles: Challenges for weather and climate models', *Bulletin of the American Meteorological Society*, 94(11), pp. 1691–1706. doi: 10.1175/BAMS-D-11-00187.1.

Kaiser, R. and Knight, W. . (1979) 'Digital signal averaging', *Journal of Magnetic Resonance (1969)*, 36(2), pp. 215–220. doi: 10.1016/0022-2364(79)90096-9.

Keller, C. A. *et al.* (2011) 'Fiber optic distributed temperature sensing for the determination of the nocturnal atmospheric boundary layer height', *Atmospheric Measurement Techniques*, 4(2), pp. 143–149. doi: 10.5194/amt-4-143-2011.

Kelly, M., Wyngaard, J. C. and Sullivan, P. P. (2009) 'Application of a Subfilter-Scale Flux Model over the Ocean Using OHATS Field Data', *Journal of the Atmospheric Sciences*, 66(10), pp. 3217–3225. doi: 10.1175/2009JAS2903.1.

Madhusudana, C. V. (2000) 'Accuracy in thermal contact conductance experiments - the effect of heat losses to the surroundings', *International Communications in Heat and Mass Transfer*, 27(6), pp. 877–891. doi: 10.1016/S0735-1933(00)00168-8.

Patton, E. G. *et al.* (2011) 'The Canopy Horizontal Array Turbulence Study', *Bulletin of the American Meteorological Society*, 92(5), pp. 593–611. doi: 10.1175/2010BAMS2614.1.

Perry, A. E. (1982) *Hot-wire anemometry*. Oxford, UK: Clarendon press.

Petrides, A. C. *et al.* (2011) 'Shade estimation over streams using distributed temperature sensing', *Water Resources Research*, 47(7). doi: 10.1029/2010WR009482.

Sayde, C. *et al.* (2014) 'Mapping variability of soil water content and flux across 1-1000 m scales using the Actively Heated Fiber Optic method', *Water Resources Research*, 50(9), pp. 7302–7317. doi: 10.1002/2013WR014983.

Sayde, C. *et al.* (2015) 'High-resolution wind speed measurements using actively heated fiber optics', *Geophysical Research Letters*, 42(22), pp. 10064–10073. doi: 10.1002/2015GL066729.

Schilperoort, B. *et al.* (2018) 'Technical note: Using distributed temperature sensing for Bowen ratio evaporation measurements', *Hydrology and Earth System Sciences*, 22(1), pp. 819–830. doi: 10.5194/hess-22-819-2018.

Selker, J. *et al.* (2006a) 'Fiber optics opens window on stream dynamics', *Geophysical Research Letters*, 33(24), pp. 27–30. doi: 10.1029/2006GL027979.

Selker, J. S. *et al.* (2006b) 'Distributed fiber-optic temperature sensing for hydrologic systems', *Water Resources Research*, 42(12), pp. 1–8. doi: 10.1029/2006WR005326.

Steele-Dunne, S. C. *et al.* (2010) 'Feasibility of soil moisture estimation using passive distributed temperature sensing', *Water Resources Research*, 46(3). doi: 10.1029/2009WR008272.

Taylor, G. I. (1938) 'The Spectrum of Turbulence', *Proceedings of the Royal Society A: Mathematical, Physical and Engineering Sciences*, 164(919), pp. 476–490. doi: 10.1098/rspa.1938.0032.

Thomas, C. K. *et al.* (2012) 'High-Resolution Fibre-Optic Temperature Sensing: A New Tool to Study the Two-Dimensional Structure of Atmospheric Surface-Layer Flow', *Boundary-Layer Meteorology*, 142(2), pp. 177–192. doi: 10.1007/s10546-011-9672-7.

Tsilingiris, P. T. (2008) 'Thermophysical and transport properties of humid air at temperature range between 0 and 100°C', *Energy Conversion and Management*, 49(5), pp. 1098–1110. doi: 10.1016/j.enconman.2007.09.015.

Tyler, S. W. *et al.* (2008) 'Spatially distributed temperatures at the base of two mountain snowpacks measured with fiber-optic sensors', *Journal of Glaciology*, 54(187), pp. 673–679. doi: 10.3189/002214308786570827.

Tyler, S. W. *et al.* (2009) 'Environmental temperature sensing using Raman spectra DTS fiber-optic methods', *Water Resources Research*, 45(4), pp. 1–11. doi: 10.1029/2008WR007052.

Webster, C. A. G. (1962) 'A note on the sensitivity to yaw of a hot-wire anemometer', *Journal of Fluid Mechanics*, 13(02), p. 307. doi: 10.1017/S0022112062000695.

Zeeman, M. J., Selker, J. S. and Thomas, C. K. (2015) 'Near-Surface Motion in the Nocturnal, Stable Boundary Layer Observed with Fibre-Optic Distributed Temperature Sensing', *Boundary-Layer Meteorology*, 154(2), pp. 189–205. doi: https://doi.org/10.1007/s10546-014-9972-9.

Žukauskas, A. (1972) 'Heat Transfer from Tubes in Crossflow', in, pp. 93–160. doi: 10.1016/S0065-2717(08)70038-8.